Inhibition of SREBP-mediated lipid biosynthesis and activation of multiple anticancer mechanisms by platinum complexes: Ascribe possibilities of new antitumor strategies

Xue Bai, Amjad Ali, Na Wang, Zongwei Liu, Zhimin Lv, Zeqing Zhang, Xing Zhao, Huifang Hao, Yongmin Zhang, Faiz-Ur Rahman

Inhibition of SREBP-mediated lipid biosynthesis and activation of multiple anticancer mechanisms by platinum complexes: Ascribe possibilities of new antitumor strategies

Xue Bai[a,1], Amjad Ali[b,c,1], Na Wang[a], Zongwei Liu[a], Zhimin Lv[a], Zeqing Zhang[a], Xing Zhao[a], Huifang Hao[a,d], Yongmin Zhang[a,e,*] and Faiz-Ur Rahman[a,*]

[a]Inner Mongolia University Research Center for Glycochemistry of Characteristic Medicinal Resources, Department of Chemistry and Chemical Engineering, Inner Mongolia University, Hohhot 010021, People's Republic of China

[b]Institute of Integrative Biosciences, CECOS University of IT and Emerging Sciences, Peshawar, KPK, Pakistan.

[c]Institute of Biomedical Sciences, School of Life Sciences, East China Normal University, 500 Dongchuan Road, Shanghai, 200241, People's Republic of China.

[d]School of Life Sciences, Inner Mongolia University, Hohhot 010021, People's Republic of China

[e]Sorbonne Université, CNRS, Institut Parisien de Chimie Moléculaire, UMR 8232, 4 Place Jussieu, 75005 Paris, France.

*Corresponding Authors E-mail: yongmin.zhang@upmc.fr (Y. Zhang), faiz@imu.edu.cn (F.-U. Rahman)

[1]These authors contributed equally to this work.

Abstract

Cancer is one of the most aggressive diseases with poor prognosis and survival rates. Lipids biogenesis play key role in cancer progression, metastasis and tumor development. Suppression of SREBP-mediated lipid biogenesis pathway has been linked with cancer inhibition. Platinum complexes bearing good anticancer effect and multiple genes activation properties are considered important and increase the chances for development of new platinum-based drugs. In this study, we synthesized pyridine co-ligand functionalized cationic complexes and characterized them using multiple spectroscopic and spectrophotometric methods. Two of these complexes were studied in solid state by single crystal X-ray analysis. The stability of these complexes were measured in solution state using ^{1}H NMR methods. These complexes were further investigated for their anticancer activity against human breast, lung and liver cancer cells. MTT assay showed potential cytotoxic activity in dose-dependent manner and decrease survival rates of cancer cells was observed upon treatment with these complexes. Biological assays results revealed higher cytotoxicity as compared to cisplatin and oxaliplatin. Further we studied **C2**, **C6** and **C8** in detailed mechanistic anticancer analyses. Clonogenic assay showed decrease survival of MCF-7, HepG2 and A549 cancer cells treated with **C2**, **C6** and **C8** as compared to control cells treated with

DMSO. TUNEL assay showed more cell death, these complexes suppressed invasion and migration ability of cancer cells and decreased tumor spheroids formation, thus suggesting a potential role in inhibition of cancer metastasis and cancer stem cells formation. Mechanistically, these complexes inhibited sterol regulatory element-binding protein 1 (SREBP-1) expression in cancer cells in dose-dependent manner and thereby reduced lipid biogenesis to suppress cancer progression. Furthermore, expression level was decreased for the key genes LDLR, FASN and HMGCR, those required for sterol biosynthesis. Taken together, these complexes suppressed cancer cell growth, migration, invasion and spheroids formation by inhibiting SREBP-1 mediated lipid biogenesis pathway.

Keywords

Platinum complexes, Anticancer study, SREBP-1 inhibition, Cell invasion, Cancer cell migration, Cancer cells stemness.

1. Introduction

Clinically approved platinum-based anticancer drugs including cisplatin, carboplatin, nedaplatin, heptaplatin, lobaplatin and oxaliplatin (Figure 1) have been used worldwide in chemotherapy of cancer patients with multiple types of solid tumors [1-3]. Among them the first drug approved was cisplatin that showed great clinical successes in treatment of cancer patients and improved the survival rate of cancer patients [4-8]. The approval of cisplatin as a drug and use in chemotherapy also revealed multiple drawbacks including neurotoxicity, nephrotoxicity, vomiting, ototoxicity, loss of sensation in the hands, haemolysis, bone marrow suppression etc. in cancer patients [9-13]. Therefore, multiple researches were carried out on this metal-based drug and with the passage of time other platinum-based anticancer drugs were approved for clinical use to decrease the drawbacks associated with cisplatin. In all these drugs the most common active function was square planner platinum metal while the coordinating assembly was modified and these changes in assembly overcame several drawbacks of cisplatin [1, 14-17]. These Pt(II)-based drugs showed good efficacy in multiple types of cancer patient. Inspired form these strategies, several studies are being carried out to develop novel assembly based Pt(II) anticancer complexes. The structure of the ligand and its attached functional groups play crucial roles in the efficiency as well as the reduction of side effects of the newly reported platinum-based anticancer complexes [1, 14, 15, 18]. New complexes were reported with different structural aspects including new ligand, biomolecules derived ligands, biomolecules functionalized ligands or assembly prepared from an already used drug [19-21]. The incorporation of such coordinating ligand improved the chemotherapeutic effect and minimized the

side effects. Similarly modification in these assembly added modification to their mode of actions or targets of several platinum complexes [22-25]. The assembly with biomolecules resulted in safety or targeted delivery while functionalization with an already used drug empowered synergy and efficacy [26-28]. All these mentioned approaches are supposed to increase the choices for new platinum drug development investigations that will increase the survival rate of cancer patients. These outcomes increased the interests of modern researchers in the investigation of platinum complexes with easy synthesis, solubility, stability, targeted, with lower side effects, favorable toxicity etc. [22, 28-30].

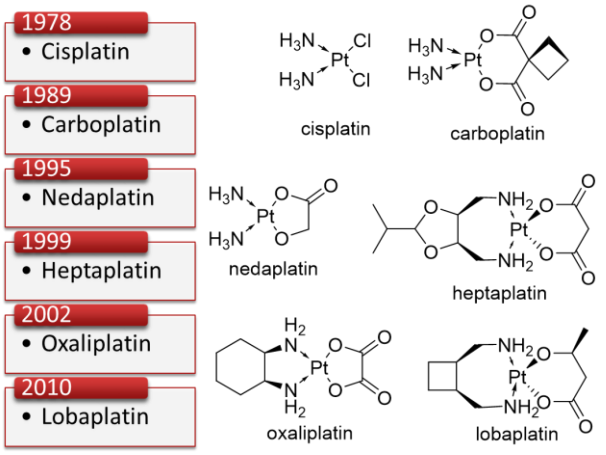

Figure 1 Clinically used platinum-based anticancer drugs with year of approval

Lipids biosynthesis plays key roles in cancer progression, cancer cell proliferation and survival. Increased lipids production is linked with the proliferation of tumor cells and lipids also play important roles in the activation of signaling pathways that are required for tumor development. Lipids biogenesis also help in the production of ATP that is mainly utilized by cancer cells to accelerate cancer progression. Thus lipids biogenesis and fatty acid synthesis are considered important in tumor development, metastasis and invasion. Several studies showed that lipids biogenesis is highly activated in tumor cells [31, 32]. Sterol regulatory element-binding protein 1 (SREBP-1) is a transcription factor that plays critical roles in lipids biogenesis and fatty acid synthesis. High expression of SREBP-1 is correlated with cancer progression and cancer cells proliferation, thus several studies showed elevated expression of SREBP-1 in human cancers. Depletion of SREBP-1 has been linked with decreased lipids biogenesis and fatty acid synthesis and thereby decreases cancer cells growth and increase apoptosis. Several oncogenic signaling pathways such as AKT and PI3K have been shown to activate SREBP-1 in cancer cells. Elevated levels of SREBP-1 positively correlated with tumor metastasis and predict poor survival rates in cancer patients [31, 33-35].

Tumors are heterogeneous in nature and possess different genetic and epigenetic changes. Invasion and migration play key roles in cancer metastasis. Both invasion and migration are considered critical steps for cancer cells to metastasize from primary site to secondary site [36, 37]. Cancer stem cells formation increases drug resistance and tumorsphere formation is also associated with increased cancer progression [38]. However, different types of cancer cells are highly dependent on lipids, proteins and nucleic acids for their growth, invasion, migration, metastasis and proliferation. To meet the requirement of increased lipids cancer cells often enhanced lipids biogenesis and fatty acid synthesis [39, 40].

In search of novel and potent anticancer agents several modifications were made in the already market available Pt(II) drugs like cisplatin or oxaliplatin. [21, 22, 41] Still a clear rationale about structure activity relationship (SAR) was not established to show which kinds of ligands will have better effect on the anticancer properties, in difference studies only the SAR of closely related ligands derived Pt(II) complexes was deduced. [42] In this scenario the only approach to hunt for the most effective Pt(II) anticancer complexes was the synthesis and biological analyses of large numbers of assemblies based Pt(II) complexes. We investigated many salicylaldimine type of ligands derived metal complexes and checked their anticancer properties. [43-51] The anticancer properties of all those complexes were comparable to cisplatin. Among them the most effective class of complexes observed was the SNO donor salicylaldimine ligand derived Pt(II) complexes. [43, 44] We are further working on their modifications to search other related isomers those could be easily synthesized and show enhance anticancer effect as compared to already used platinum anticancer drugs.

We recently reported platinum anticancer complexes [43] with potent anticancer activities, in this study these complexes were further modified with co-ligand pyridine. This modification further increased the anticancer potentials of these complexes. All these complexes were thoroughly characterized by multiple analytical techniques and two complexes were analyzed in solid state by single crystal X-ray structure analysis. These complexes were studied for their stability by ^{1}H NMR spectroscopy and their anticancer effects was studied in multiple human cancer cells including MCF-7, HepG2 and A549 cells. Several mechanistic studies of their anticancer effects were performed including cell migration and invasion, cancer stem cells/tumor spheroids formation, inhibition effect on the clonogenic potential of cancer cells, lipids biogenesis and fatty acid synthesis by targeting SREBP-1 dependent signaling pathway and LDLR, FASN and HMGCR genes expressions. The anticancer effect was compared to market available Pt(II)-based anticancer drugs cisplatin and oxaliplatin.

2. Results

2.1. Chemistry

*2.1.1 Synthesis and characterization of **C1-C8***

Each complex (**C1-C8**) was prepared from the precursor complex (**PC1-PC8**) [43], the ancillary chloride ligand was abstracted using $AgBF_4$ in acetonitrile and successively treated with excess pyridine (co-ligand) to get **C1-C8** in excellent isolated yields. These complexes were structurally characterized by ^1H, ^{13}C NMR, UV-vis and FT-IR spectroscopy and HR-ESI mass spectrometry (ESI Figure S1-S33). For **C1-C8** the main difference in the ^1H NMR spectra compared to the precursor complexes, the most downfield shift was assigned to the imine proton and found in the region 9.88 – 9.55 ppm. Three new chemical shifts one doublet in the second most downfield area of the aromatic regions 9.14 - 8.81 ppm was observed for two protons at 2 position of the co-ligand pyridine while the remaining chemical shifts were hard to be assigned due to mixing with the salicylaldimine ligands protons signals. Compared to the precursor complexes each carbon signal was shifted up or down field depending on its position and proximity to Pt(II) center.

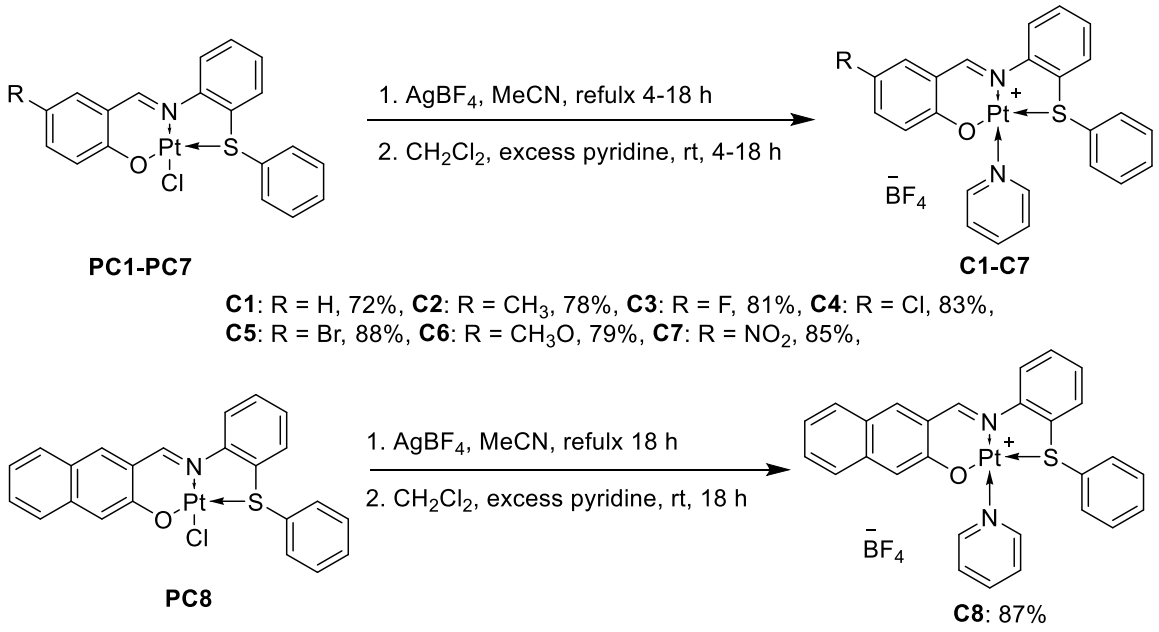

Scheme 1 Synthetic scheme for **C1**–**C8**

*2.1.2. UV-vis spectroscopic study of **C1-C8***

The UV-vis absorption spectra of **C1-C8** were recorded in chloroform solution at rt, all the spectra were plotted in Figure 2. The main absorption peaks for **C1-C6** were found around 250 and 330 nm regions were assigned to ligand-to-ligand (LLCT), similarly the absorption peaks for **C1-C3** and **C5-C6** around 460 nm while for **C4** it was found at 480 nm, were assigned to metal-to-ligand charge transfer (MLCT) transitions. These complexes showed similarity in their UV-vis absorption wavelengths. **C7** showed blue

shift in all these peaks and displayed absorption around 250, 315 and 435 nm could be due to the strong electron withdrawing effect of the nitro group attached to the salicylaldimine ligand. In case of **C8** these peaks were observed around 255, 370 and 475 nm showing red shift that could be due to the electron rich naphthalene ring of the salicylaldimine ligand. MLCT of all these complexes were lower in energy thus observed in the visible region of the UV-vis spectra.

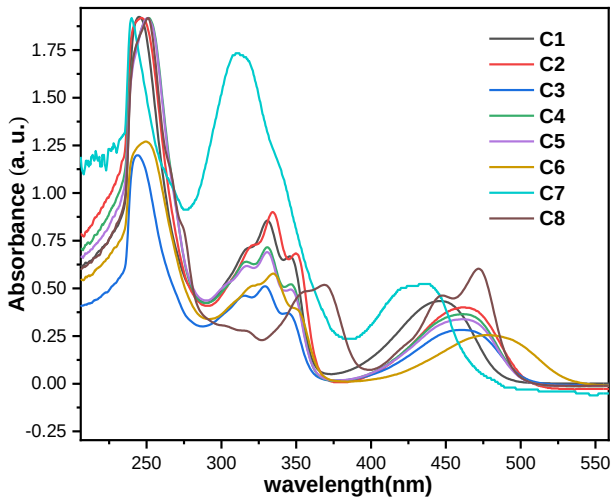

Figure 2 UV-vis absorption spectra plot of **C1-C8**

*2.1.3. FT-IR spectroscopic study of **C1-C8***

FT-IR analysis for each **C1-C8** was performed using KBr pellet dilution method, the comparative spectra plot is displayed in Figure 3 and ESI Figure S25 –S33. In the IR spectrum, different peaks were assigned according to the previously reported literature. In each **C1-C8**, aromatic C-H stretching was assigned around 3020-3059 cm^{-1}, C=C stretching around 1548-1444 cm^{-1} and C=N around 1400-1376 cm^{-1}. The biggest and broad peak around 1070-1045 cm^{-1} in each complex was assigned as stretching frequency of BF_4 anions. The main difference in the IR spectrum of each complex to its precursor complex was the presence of this big broad BF_4 anions peak, this also confirmed the exchanges of Cl to BF_4 (ESI Fig. S25).

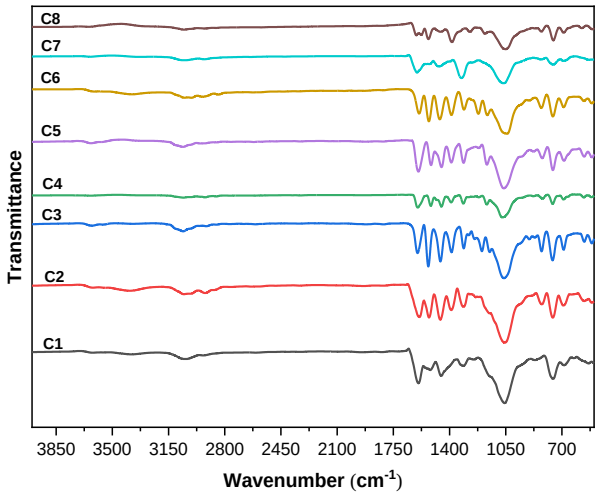

Figure 3 FT-IR spectra plot of **C1-C8**

*2.1.4. Single crystal description of **C1** and **C3***

X-ray quality crystals of each **C1** and **C3** were obtained by slow evaporation of CH_2Cl_2–*n*-hexane solutions. Single crystal structure data were plotted in Figure 4 (**C1**) and Figure 5 (**C3**). Similarly, the crystal structure parameters were tabulated in Table 1. **C1** crystallized in monoclinic while **C3** in triclinic crystal system where Pt(II) adopted square planner environment. In both of these crystals the coordinated functions were SNO atoms of main salicylaldimine ligand in which O atom was covalently bonded while SN were coordinate covalently bonded to Pt(II) metal [43]. The fourth coordinate of Pt(II) was completed by N donor atom of co-ligand pyridine that was coordinate covalently bonded to metal (Figure 4 and 5). Bond lengths and angles around Pt center in **C1** and **C3** were shown in Figure 4B, 5B and Table 2. The bond lengths and bond angles in both **C1** and **C3** were almost similar (Table 2 entry 1–10). Pt(1)-S(1) bond length was the longest in each complex as compared to the bond length between Pt(II) and other atoms and found to be 2.2328(17) and 2.236(2) for **C1** and **C3** respectively (Table 2 entry 4), while the shortest bond length was Pt(1)–O(1) in **C1** while Pt(1)-N(1) in **C2** (Table 2 entry 1 and 2). The other bond lengths were almost similar in both of these complexes. The bond angles with different coordinated atoms around Pt(II) center were almost similar in both of these complexes. Bond angle formed by ∠O(1)-Pt(1)-N(2) was observed to be the smallest while ∠O(1)-Pt(1)-N(1) was the biggest one among all angles in **C1** and **C2** (Table 2 entry 5 and 6). Ligand around Pt(II) center got planner symmetry and inter plane stacking was observed in each complex.

In crystal packing of each complex multiple short interactions were observed (Figure 4C and Figure 5C) with different bond lengths (Figure 4D and Figure 5D). Similarly inter-planer interactions resulted in the

formation of 1D chains in crystal packing (Figure 4E and Figure 5E), those were cemented by multiple short interactions to the other neighbouring 1D chains to form 3D arrangement in crystal packing.

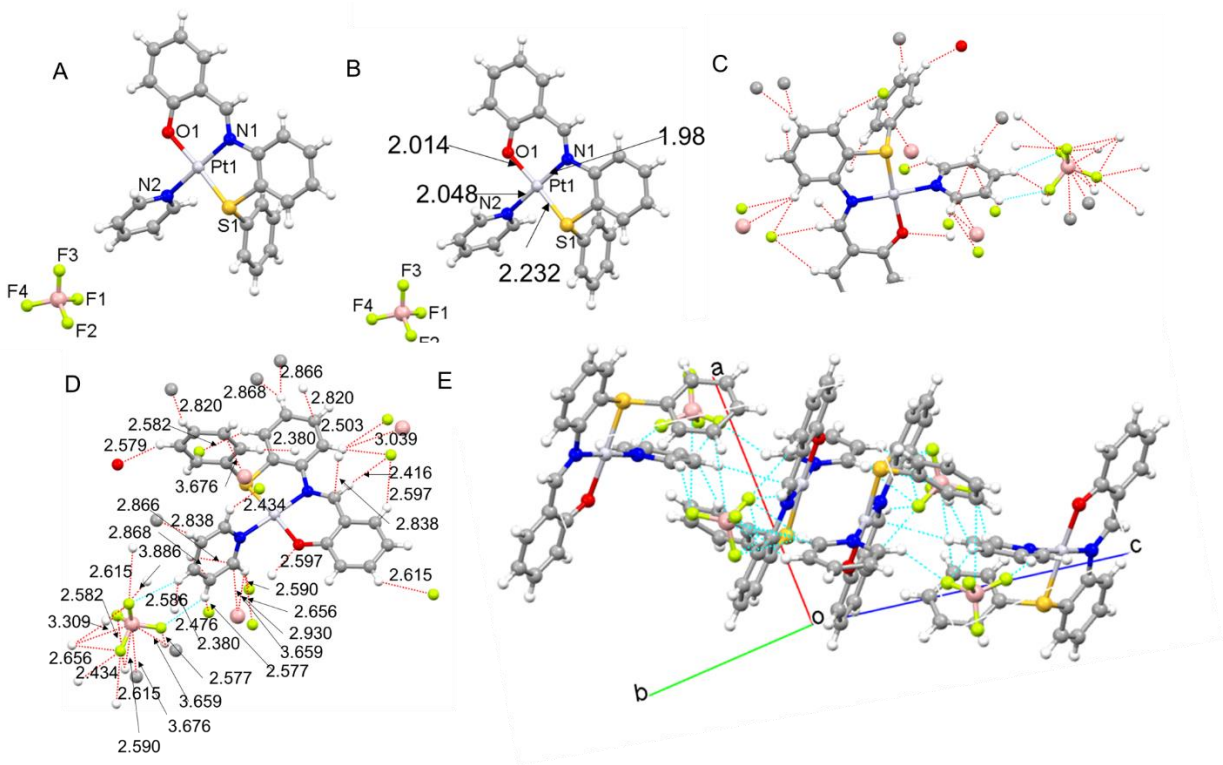

Figure 4. Single crystal data plot of **C1** (A) single molecule plot showing atoms around Pt(II) center (B) bond lengths between Pt and coordinated atom (C) plot showing close contacts with neighboring molecules (D) plot showing distances of close contacts (E) arrangement of molecules in 1D manner in crystal packing.

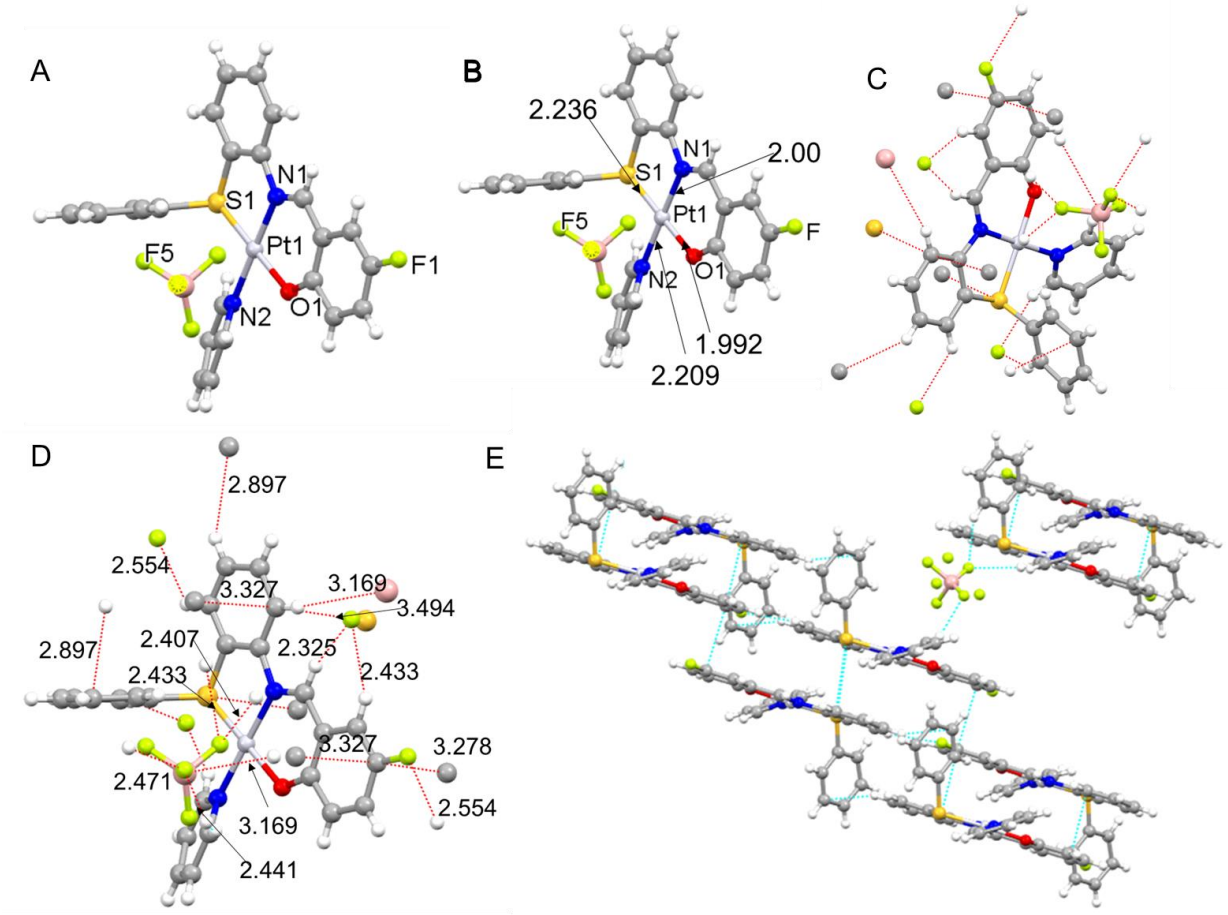

Figure 5. Single crystal data plot of **C3** (A) single molecule plot showing different atoms attached to Pt (B) bond lengths between Pt and attached atom (C) plot showing close contacts with neighboring molecules (D) plot showing distances of these close contacts (E) arrangement of molecules in 1D manner in crystal packing.

Table 1 Structure refinement parameters of **C1** and **C3**

	C1	**C3**
Empirical formula	$C_{24}H_{19}BF_4N_2OPtS$	$C_{24}H_{18}BF_5N_2OPtS$
Formula weight	665.37	683.36
Temperature (K)	203(2)	203(2)
Crystal system	Monoclinic	Triclinic
Space group	$P2_1/n$	P-1
Unit cell dimensions		
a (Å)	10.2689(17)	9.3700(12)
b (Å)	15.510(3)	9.6514(12)
c (Å)	14.174(2)	14.4197(18)
α (°)	90	77.539(2)
β (°)	97.853(3)	85.187(2)
γ (°)	90	83.671(2)

Volume ($Å^3$)	2236.3(6)	1263.1(3)
Z	4	2
Density (calculated) (mg/m^3)	1.976	1.797
Absorption coefficient (mm^{-1})	6.422	5.693
F(000)	1280	656
Crystal size (mm^3)	0.800 x 0.650 x 0.450	0.320 x 0.170 x 0.130
Theta range for data collection (°)	1.956 to 27.997	2.171 to 25.995
Index ranges	-13<=h<=13, -20<=k<=20, -16<=l<=18	-11<=h<=11, -11<=k<=10, -17<=l<=14
Reflections collected	15941	8097
Independent reflections	5389 [R(int) = 0.0496]	4869 [R(int) = 0.0235]
Data / restraints / parameters	5389 / 0 / 307	4869 / 55 / 344
Goodness-of-fit on F^2	1.089	0.990
Final R indices [I>2sigma(I)]	R1=0.0486,wR2= 0.1360	R1 = 0.0403, wR2 = 0.1198
R indices (all data)	R1=0.0542,wR2= 0.1417	R1 = 0.0481, wR2 = 0.1525
Largest diff. peak and hole ($e.Å^{-3}$)	2.147 and -6.045	1.444 and -1.232

Table 2. Selected bond lengths (Å) and angles (°) around Pt atom in each complex

Entry	**Bond/Angle**	**C1**	**C3**
Bond length (Å)			
1	Pt(1)-O(1)	2.014(5)	1.992(6)
2	Pt(1)-N(1)	1.985(5)	2.001(7)
3	Pt(1)-N(2)	2.048(5)	2.029(7)
4	Pt(1)-S(1)	2.2328(17)	2.236(2)
Bond angle (°)			
5	∠O(1)-Pt(1)-N(1)	94.96(18)	93.8(3)
6	∠O(1)-Pt(1)-N(2)	85.1(2)	84.9(3)
7	∠N(1)-Pt(1)-N(2)	177.0(2)	178.6(3)
8	∠O(1)-Pt(1)-S(1)	175.99(14)	176.92(18)
9	∠N(1)-Pt(1)-S(1)	87.12(15)	87.62(19)
10	∠N(2)-Pt(1)-S(1)	92.99(17)	93.7(2)

2.1.5. Stability of reference complexes in solution state

Platinum complexes are susceptible to good donor solvents e.g. acetonitrile or DMSO etc., these solvents usually replace labile or easily displaceable ligand from Pt(II) center and affect the biological activity of a particular platinum anticancer complex. Most of the metal based complexes show low or no solubility in water so their stock solutions are prepared in dimethyl sulfoxide (DMSO) during their *in vitro* or *in vivo* biological screening. DMSO is reported as least compatible solvent for preparation of solution of cisplatin and other Pt-based drugs and reported to decrease the anticancer activity of all these market available drugs [52]. Similarly aquation of platinum anticancer complexes in the presence of water in which the labile ligand is exchanged by water thus resulting in aquated complexes also affect the biological effect of platinum complexes [53, 54]. The main target of a platinum complex is DNA that reside inside the nucleus, where platinum metal interact with DNA by crosslinking, mono adduct formation or intercalating double DNA strand to stop DNA replication and cause apoptosis [21, 55-58]. Therefore the stability of platinum complexes in solution state in particular solvents is important, that could be investigated easily by ^{1}H NMR spectroscopy through repeated time dependent analyses.

The stability of **C4**, **C6**, **C7** and **C8** as reference complexes was analyzed by ^{1}H NMR spectroscopy in 15% D_2O/DMSO-d_6 conducting time dependent repeated analyses (ESI Figure S34-S37). These analysis conducted over 7 days showed no changes in the main protons chemical shifts of each of these complexes. Thus, suggesting these complexes to be highly stable in solution state in this solvent system and it could also be the reason of their potential anticancer effect.

Stability analyses for reference complexes **C4** and **C6** were also conducted in pure D_2O over 7 days; for the purpose each **C4** or **C6** bearing BF_3 anions was dissolved in minimum amount of acetonitrile and 2 equivalents of tetrabutylammonium chloride was added to it. The mixture was stirred for 30 minutes and added with excess diethyl ether. The solid precipitate was filtered, washed with ether and dried. 1 mg of the solid **C4** or **C6** was dissolved in 0.5 mL of D_2O and subjected to ^{1}H NMR analyses. The comparative plot over time for **C4** (ESI Fig. 38) and **C6** (ESI Fig. 39) showed no changes in the main protons signals showing these compounds are stable in water. This analysis confirmed the uniformity of each of these complex over the mentioned time in water solution.

2.2. Biology

2.2.1. Anticancer effects in cancer cells

The cell growth inhibition effect of **C1-C8** was tested on human breast cancer (MCF-7), human liver cancer (HepG2) and human lung cancer (A549) cell lines. Cancer cells were treated with 20 μM of each complex for 48 h and MTT assay was performed. MTT assay results showed that **C2**, **C6** and **C8** were highly potent in these cancer cell lines in comparison to other counterparts in this group of complexes

(Figure 6A). Next, the effect of increasing concentration on the viability of cancer cells was also analyzed by MTT assay. MCF-7, HepG2 and A549 cancer cells were treated with 2.5, 5, 10 or 20 µM of **C2**, **C6** or **C8** for 48 h and analyzed for their cell growth inhibition. MTT assay results showed dose-dependent inhibition in growth of these cancer cells (Figure 6B-6D). These results suggested **C1**-**C8** have significant anticancer activity against these cancer cells and their anticancer effects are exerted in dose-dependent manner.

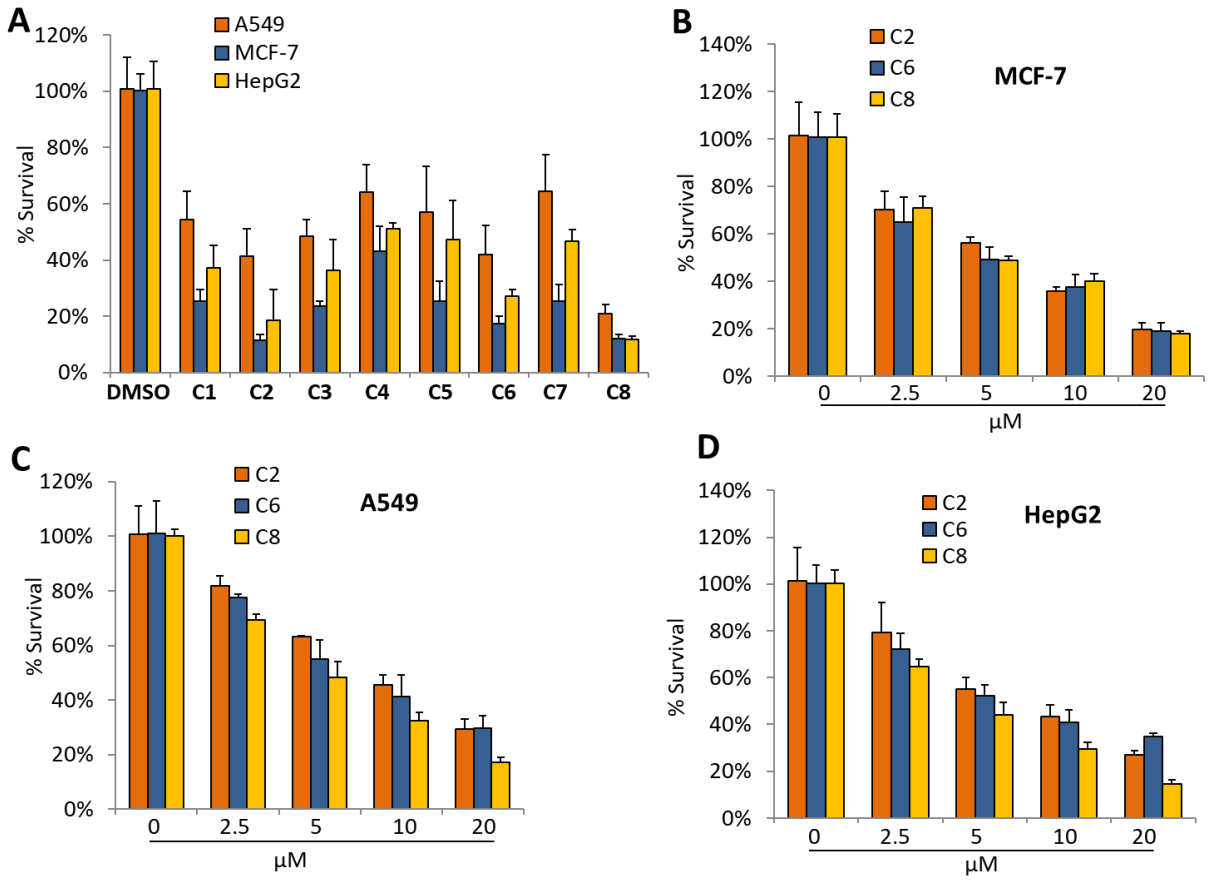

Figure 6 Human cancer cells growth inhibition; (A) A549, MCF-7 and HepG2 cancer cells were treated with DMSO and (**C1**-**C8**) (20 µM for 48 h and analyzed by MTT assay for cell viability, (B-D) MCF-7, A549 and HepG2 cancer cells were treated with 0, 2.5, 5, 10 and 20 µM of **C2**, **C6** and **C8** for 48 h and cell viability was analyzed by MTT assay.

*2.2.2. Comparative anticancer effect of **C2**, **C6** and **C8** with cisplatin and oxaliplatin*

The anticancer effect of **C2**, **C6** and **C8** was compared with market available drug cisplatin and oxaliplatin in MCF-7, HepG2 and A549 cancer cells. We observed that **C8** was much more potent than cisplatin and oxaliplatin in these cancer cells, while **C2** and **C6** cytotoxic effect was nearly equal to

cisplatin but much better than oxaliplatin (Figure 7A and 7B). These results showed comparative cytotoxic effect of these complexes to market available drugs and suggested **C8** to be much more cytotoxic in MCF-7, HepG2 and A549 cells, thus highlighting the importance of **C8** in treatment of cancer cells.

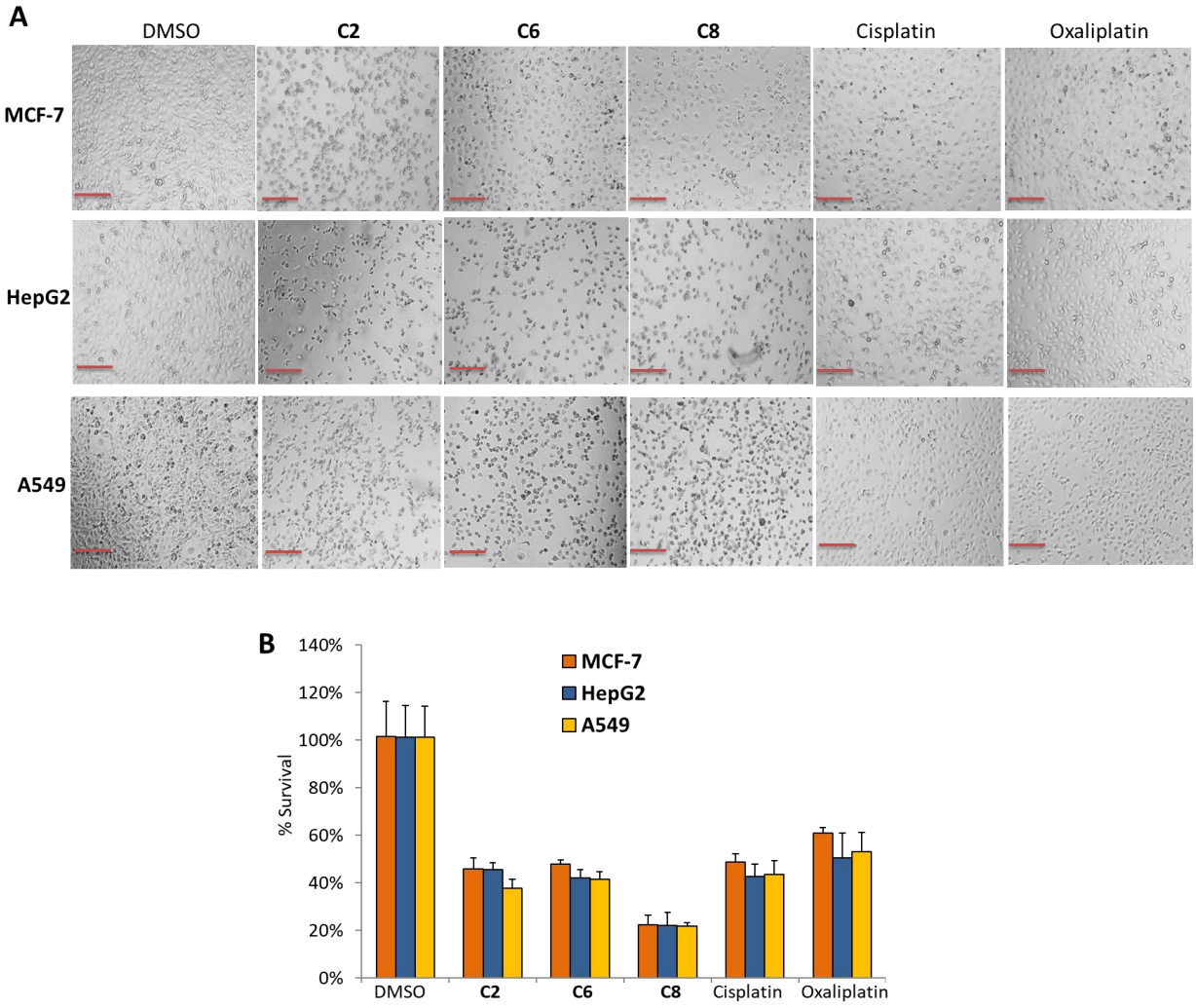

Figure 7 Comparison of cytotoxic activity of **C1-C8** with cisplatin and oxaliplatin in cancer cells; (A) Bright field images of A549, MCF-7 and HepG2 cancer cells treated with DMSO or 20 µM of **C2**, **C6**, **C8**, cisplatin or oxaliplatin for 48 h and bright field images were taken (Magnification 20X) (B) A549, MCF-7 and HepG2 cancer cells treated with DMSO or 20 µM of each mentioned complex for 48 h and analyzed by MTT assay for cell viability.

*2.2.3. Suppression of clonogenic potential of cancer cells induced by **C2**, **C6** and **C8***

Similarly, the effect of **C2**, **C6** and **C8** was investigated on long-term clonogenic cancer cells growth. MCF-7, HepG2 and A549 cells were treated with 2.5, 5, 10 and 20 µM of **C2**, **C6** or **C8** for 48 h and then media containing drug were removed from cell lines. MCF-7, HepG2 and A549 cancer cells were grown for next 12 days in drug free media and crystal violet assay was performed. The results showed strong inhibition in clonogenic growth of cancer cells treated with **C2**, **C6** or **C8** as compared to the control cell lines (Figure 8A-8C). The result of crystal violet assay data suggested that these complexes has the ability to suppress clonogenic potential of cancer cells.

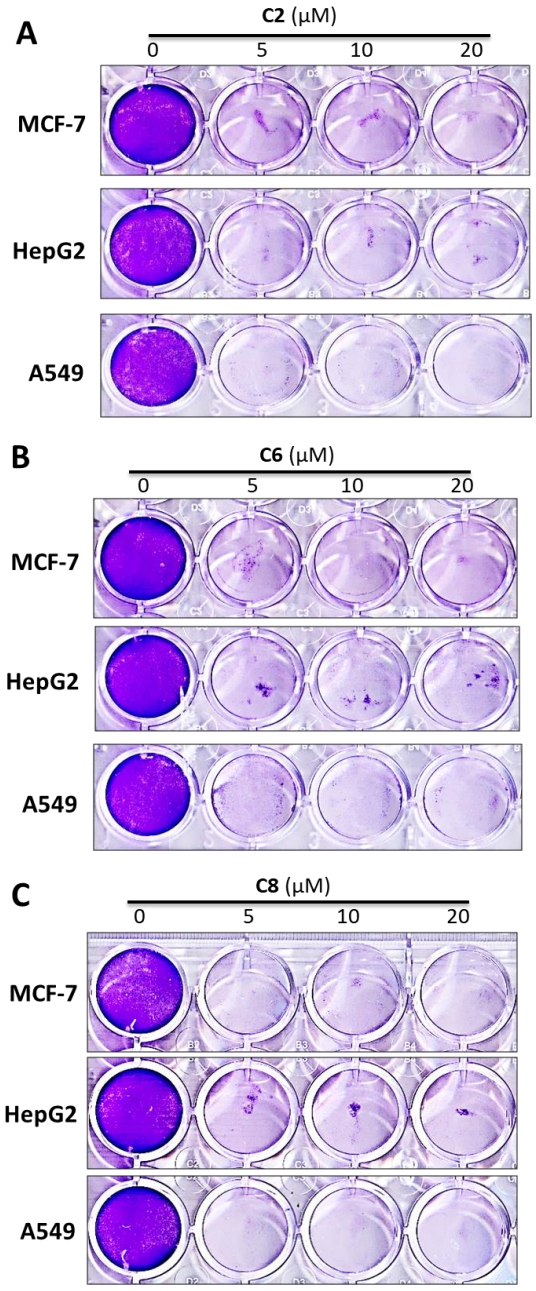

Figure 8 Pt(II) complexes inhibit clonogenic potential of cancer cells; (A-C) A549, MCF-7 and HepG2 cells were treated with 5, 10 or 20 μM of **C2**, **C6** or **C8** for 48 h and then further maintained in drug free medium for 12 days to determine clonogenic potential of cancer cells.

2.2.4. Cancer cells death analysis using TUNEL assay

Next, cancer cell death induced by selected complexes (**C2**, **C6** and **C8**) was investigated by TUNEL assay. MCF-7, HepG2 and A549 cells were treated with 20 μM of **C2**, **C6** or **C8** for 48 h and then analyzed by TUNEL assay. TUNEL assay showed induction of cell death in MCF-7, HepG2 and A549

cancer cells treated with each of these complexes as compared to the control cell lines treated with DMSO (Figure 9A and 9B). Taken together, these results showed the potentials of these complexes to induce cancer cell death and thereby reduce cell viability.

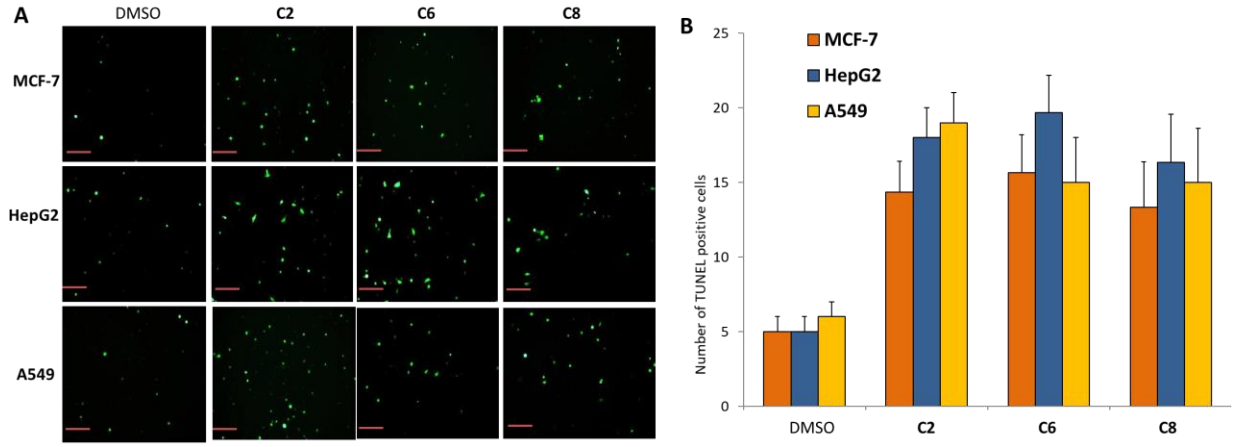

Figure 9 Pt(II) complexes induce cancer cell death; (A) MCF-7, HepG2 and A549 cancer cells were treated with 20 µM of **C2**, **C6** or **C8** for 48 h and cell death was analyzed by TUNEL assay (Magnification 20X) (B) Graphical data represent statistical analysis from figure A.

2.2.5. Cancer cells migration induced by Pt(II) complexes

Cancer cell migration plays critical roles in cancer progression by helping cancer cells to migrate from primary site to secondary site which finally leads to metastasis. Suppression of cancer cell migration is connected with cancer inhibition [36, 37]. Therefore, we investigated the effect of these complexes on cancer cells migration using wound healing assay. MCF-7, HepG2 and A549 cells were treated with 20 µM of **C2**, **C6** or **C8** for 24 h and the migration ability of these cancer cells was determined through wound healing assay. Results showed that cancer cells treated with **C2**, **C6** or **C8** were less migrated in compassion to the control cells treated with DMSO in other word control cells were much faster migrated than treated cell lines (Figure 10A-10C). Taken together, wound healing assay showed that these complexes have strong potentials to suppress migration of cancer cells.

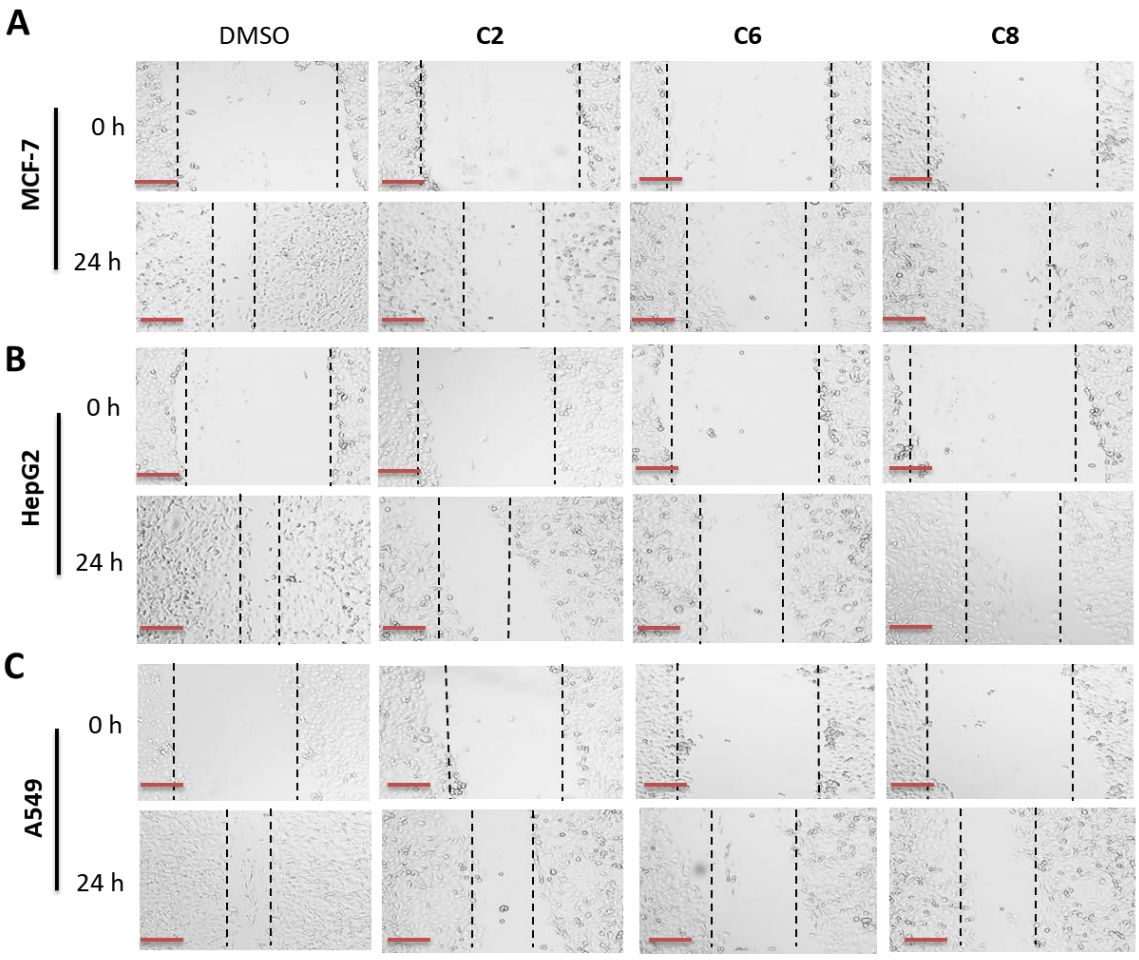

Figure 10 Effect on cancer cells migration; (A-C) MCF-7, HepG2 and A549 cells were treated with 20 µM of **C2**, **C6** or **C8** for 24 h and then wound healing assay was performed for 24 h to determine wound healing area (Magnification 20X).

2.2.6. Suppression of cancer cells invasion

Invasion of cancer cells into blood stream from cancer tissues play a major role in cancer progression and cancer metastasis. Inhibition of cancer cells invasion has been linked with decrease metastatic potential [36, 37]. The effect of these of Pt(II) complexes on the invasion ability of cancer cells was investigated, MCF-7, HepG2 and A549 cancer cells were treated with 20 µM of **C2**, **C6** or **C8** for 24 h and invasion ability of these cancers were determined through invasion chambers. Results showed less invasion of cancer cells treated with **C2**, **C6** or **C8** as compared to the control cells that treated with DMSO (Figure 11A-11B). These results demonstrated that these complexes to have good potentials to decrease the invasive ability of cancer cells.

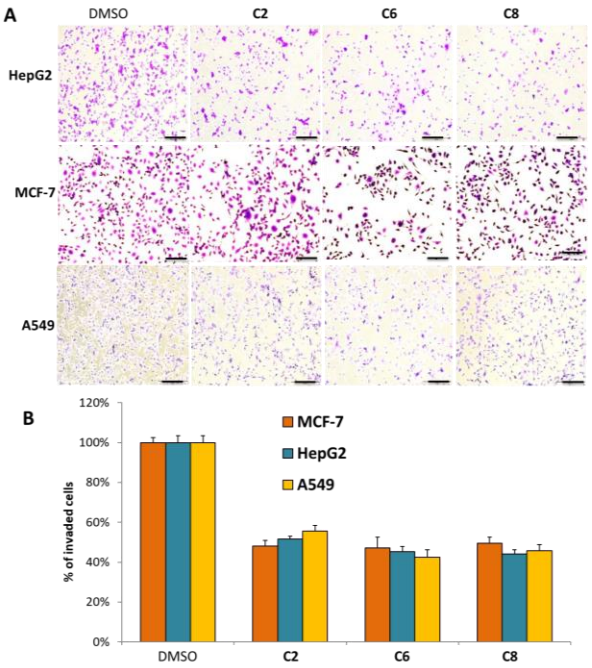

Figure 11 Cancer cells invasion study; (A-C) MCF-7, HepG2 and A549 cancer cells were treated with 20 µM of **C2**, **C6** or **C8** for 48 h and invasion ability was determined by cell invasion assay (Magnification 20X) (B) Graphical data represent statistical analysis from figure A.

2.2.7. Suppression of cancer stem cells formation

Cancer stem cells formation plays key roles in cancer progression, therapeutic resistance, cancer cells survival and clonal evolution. Cancer stem cells often show resistance to chemotherapy and thereby make the anticancer agents less effective against cancer progression [38]. Therefore, we investigated the effect of **C2**, **C6** and **C8** on cancer stem cells/tumor spheroids formation. MCF-7, HepG2 and A549 cells were grown as tumorsphere in ultralow attachment plates and then treated with **C2**, **C6** or **C8** for 7 days. Imaging analysis of cancer stem cells formation showed that there was significant inhibition in spheroids formation in cancer cells treated with Pt(II) complexes as compared to the control cells (Figure 12A-12B). These results showed that **C2**, **C6** and **C8** have the ability to decrease cancer stem cells/tumor spheroids formation and thereby suppress cancer progression.

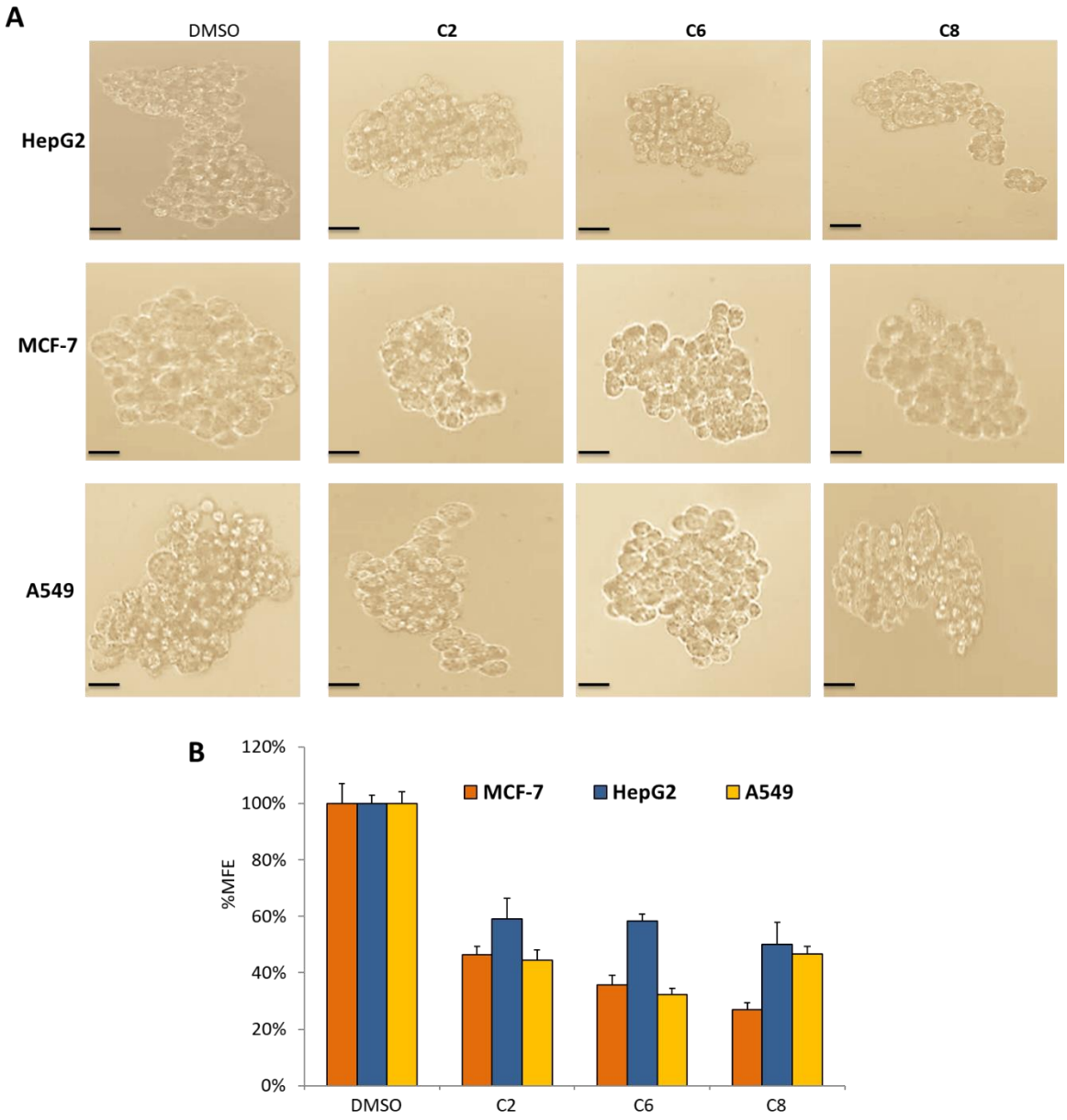

Figure 12 Inhibition of spheroids formation of cancer cells induced by Pt(II) complexes; (A) HepG2, MCF-7 and A549 cancer cells were treated with 20 µM of **C2**, **C6** or **C8** for 7 days and cancer stem cells ability was determined by spheroids assay in ultra-low attachment plates (Magnification 20X) (B) Graphical data represent percentage mammosphere formation efficiency (% MFE) from figure A.

2.2.8. Pt(II) complexes suppress lipid biogenesis via SREBP-1 dependent pathway

Sterol regulatory element-binding protein 1 (SREBP-1) play a critical role in lipid biogenesis and thereby promote cancer progression and metastasis. SREBP-1 has been shown to promote cancer cells growth and depletion of SREBP-1 is linked with cancer inhibition. SREBP-1 signaling is important for lipid

biogenesis and lipid biogenesis has been linked with tumor development [31]. Therefore, we investigated the effect of the most potent complex **C8** on SREBP-1 dependent signaling pathway. MCF-7, HepG2 and A549 cancer cells were treated with 5, 10 or 20 µM of **C8** and SREBP-1expression was analyzed by western blot. Western blot analysis showed dose-dependent inhibition of SREBP-1expression in MCF-7, HepG2 and A549 cells treated with **C8** as compared to the control cell treated with DMSO (Figure 13A). Taken together, these results suggested that **C8** has stronger ability to repress SREBP-1 expression in cancer cells and thereby reduce lipids biogenesis.

Next we also tested the effect of **C8** on LDLR (Low Density Lipoprotein Receptor), FASN (Fatty Acid Synthase) and HMGCR (3-Hydroxy-3-Methylglutaryl-CoA Reductase), those play central role in fatty acid/cholesterol biosynthesis. SREBP-1 knockdown has been linked with the decrease expression of LDLR, FASN and HMGCR. As our results showed inhibition in SREBP-1 expression in response to **C8**, therefore we also investigated the effect of this complex on the expressions of LDLR, FASN and HMGCR in HepG2 cells using RT-PCR analysis. Transcript analysis of LDLR, FASN and HMGCR in response to **C8** showed that this complex has the ability to suppress the expression of LDLR, FASN and HMGCR (Figure 13B), those are required for lipid biogenesis/fatty acid synthesis. Taken together, these results suggested the potential role of **C8** in the inhibition of lipid biogenesis/fatty acid synthesis by targeting SREBP-1 dependent signaling pathways and thereby reduce the expressions of LDLR, FASN and HMGCR. These results highlighted the importance of **C8** in the inhibition of lipids biogenesis and thus reduce cancer progression and cancer cell survival.

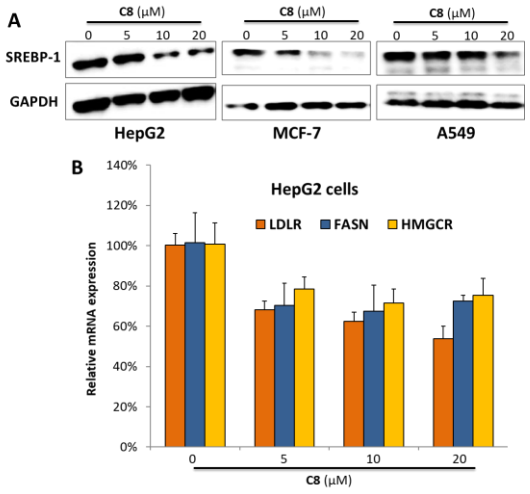

Figure 13 Pt(II) complexes inhibit SREBP-1 expression; (A) HepG2, MCF-7 and A549 cells were treated with 20 µM of **C8** for 2 days and SREBP-1 expression was determined by western blot. GAPDH was used as a loading control (B) HepG2 cells were treated with 20 µM of **C8** for 2 days and LDLR, FASN and HMGCR expressions were determined by RT-PCR.

3. Discussion

Platinum-based anticancer drugs are important chemotherapeutic candidates, comprising an estimated 50% of clinical chemotherapeutic prescriptions [2], that is due to the great successes of these drugs in cancer therapy. At the same time several limitation were found with these metal-based drugs including severe side effects in cancer patients and limitation in efficacy in all types of cancer [21]. Therefore, great attention is being paid to the synthesis and application of novel assembly-based platinum anticancer complexes to diversify this field with increasing number of choices. These novel assemblies are not only increasing the effectiveness of these drugs but also overcome several drawbacks associated with the already used market available Pt(II) based drugs. In this scenario we modified our recently reported potent platinum anticancer complexes [43] with co-ligand pyridine. This approach not only helped us obtain water solubility (with chloride anions) but stability and effectiveness as well. We synthesized **C1**–**C8** functionalized complexes that showed their ease of synthesis and also helped us establishing the exact structure using multiple analytical techniques. Their structures were well established by NMR spectroscopy, HR ESI-MS and single crystal X-ray analysis.

We reported potent anticancer platinum complexes (**C1**-**C8**) investigated *in vitro* in multiple cancer cells. The degree of the anticancer effect for **C1**-**C8** was deduced from the MTT assay and found to be in order **C8**>**C2**>>**C6**>**C1**>**C3**>**C7**>**C5**>**C4**. From the literature discussed before it is hard to conclude the exact effect of certain modifications on the anticancer effect, but it can be deduced to certain extent keeping in view the structures of different complexes in a group such as here the highest anticancer effect of **C8** and **C2**. It could be due to their modes of interaction with DNA, these complexes may form mono adduct and also intercalate DNA strand thus bind better to the target as compared to the other isomers. It is an intrinsic property of these two complexes depending upon their structures. Similarly, the lowest anticancer effect of **C4** could be due to the weaker binding to the target hindered by chlorine atom on the phenolate ring.

Lipids biogenesis and fatty acid synthesis provides fuel to cancer cells to promote migration, invasion, metastasis and cancer stem cells formation. Lipids signaling play critical role in tumor development and activation of oncogenic signaling pathways. Inhibition of lipids biogenesis is linked with decrease cancer progression. Invasion and migration of cancer cells requires ATP that is provided by several metabolic pathways including lipids signaling pathways [59-61]. SREBP-1 play critical role in cancer progression, invasion and tumor development. Decrease expression of SREBP-1 has been linked with increased apoptosis, decrease invasion and migration. Moreover, SREBP-1 plays key roles in lipid biogenesis [31]. **C1**-**C8** prepared were analyzed for the inhibition of lipid biogenesis, we studied their effect on SREBP-1

expression and other important apoptotic mechanisms. MTT assay showed high potency of these complexes against multiple human cancer cells. These complexes suppressed clonogenic potential and cancer stem cells formation. Moreover, these complexes suppressed the invasion and migration ability of cancer cells. These results highlighted the importance of these Pt(II) complexes as potential chemotherapeutic agents to target different cancer cell death mechanisms. Moreover, **C8** was found to be more potent in all these complexes, cisplatin and oxaliplatin. Different mechanisms were checked to see that how these Pt(II) complexes suppress cancer cells growth and interestingly, we found that **C8** potentially suppressed lipids biogenesis and fatty acid synthesis pathways by decreasing the expression of SREBP-1. It also inhibited the transcript levels of LDLR, FASN and HMGCR those required for fatty acid synthesis. Taken together, our results highlighted the importance of **C1-C8** in cancer inhibition by targeting SREBP-1 dependent lipid biogenesis pathway.

4. Materials and methods

4.1. Chemistry

4.1.1. General experimental and materials

All solvents and reagents were purchased from commercial sources. K_2PtCl_4 was purchased from LeYan Chemical Company China. NMR spectroscopic analyses were conducted on Bruker AVANCE 500 MHz spectrometer at 298K in DMSO-d_6 or D_2O. HR-ESI-MS spectra were acquired using waters G2-Xs QTof mass spectrometer. Crystal data was collected at 100 K on a Rigaku Oxford Diffraction Supernova Dual Source, Cu at Zero equipped with an AtlasS2 CCD using Cu Kα radiation. The data were collected and processed using Oxford Diffraction, Xcalibur CCD System. CrysAlisPro. Oxford Diffraction Ltd: Abingdon, England, UK, 201024. The structures were solved by direct methods using Olex2 software [62] and the non-hydrogen atoms were located from the trial structure and then refined anisotropically with SHELXL-2018 [63] using a full-matrix least squares procedure based on F^2. The weighted *R* factor, *wR* and goodness-of-fit *S* values were obtained based on F^2.The hydrogen atom positions were fixed geometrically at the calculated distances and allowed to ride on their parent atoms. Crystallographic data of each complex was submitted to Cambridge Crystallographic Data Center as CCDC 2096667-8, that can be obtained free of charge at e-mail: deposit@ccdc.cam.ac.uk, tel: +44-1223336408 and fax: +44-1223336003.

*4.1.2. General procedure for the synthesis of **C1–C8***

Each complex (**C1**-**C8**) was prepared from precursor complex (**PC1**-**PC8**)[43], in general 0.1 mmol of precursor complex and 0.12 mmol of $AgBF_4$ were taken in 20 mL of CH_3CN and refluxed till completion (checked by TLC eluted with 1% MeOH/CH_2Cl_2), (4-18 h). The reaction mixture was cooled to rt and filtered through celite to remove solid AgCl precipitated during the reaction. The yellow filtrate obtained was further diluted with 20 mL of CH_2Cl_2 and two drops of pyridine (co-ligand) was added to it. This mixture was stirred at rt till completion (checked by TLC 1% MeOH/CH_2Cl_2), (4-18 h) and evaporated to get a yellow or orange solid for each complex. It was recrystallized form CH_2Cl_2-n-hexane to obtain pure complex (**C1**-**C8**). Each complex was characterized thoroughly using different analytical techniques.

C1, 72% yield, light orange solid. FT- IR (KBr pellet) cm^{-1}: 3040.0，1587.6, 1444.0, 1309.9, 1055.4, 744.1, 677.1. ^{1}H NMR (500 MHz, DMSO-d_6) δ 9.64 (s, 1H), 8.86 (dt, *J* = 5.0, 1.6 Hz, 2H), 8.64 (d, *J* = 8.5 Hz, 1H), 8.20 (tt, *J* = 7.7, 1.5 Hz, 1H), 8.05 (dd, *J* = 8.1, 1.8 Hz, 1H), 7.93 (dd, *J* = 7.9, 1.4 Hz, 1H), 7.74 – 7.67 (m, 6H), 7.56 – 7.50 (m, 2H), 7.45 (dd, *J* = 8.4, 7.0 Hz, 2H), 7.07 (dd, *J* = 8.7, 1.0 Hz, 1H), 6.96 (ddd, *J* = 8.0, 6.8, 1.1 Hz, 1H) ppm. ^{13}C NMR (100 MHz, DMSO-d_6) δ 162.7, 156.8, 152.9, 152.6, 141.4, 138.3, 137.0, 133.0, 132.8, 132.4, 131.6, 130.9, 130.7, 130.6, 127.7, 127.0, 121.2, 120.4, 119.7, 118.5 ppm. HRMS (ESI): Calcd for $C_{24}H_{19}BF_4N_2OPtS$, 665.0895: Found: 578.0872 $[M\text{-}BF_4]^+$.

C2, 78% yield, light orange solid. FT- IR (KBr pellet) cm^{-1}: 3389.5, 3044.8, 2915.5, 1597.2, 1453.6, 1386.5, 1050.6, 825.5, 748.9, 681.9. ^{1}H NMR (500 MHz, DMSO-d_6) δ 9.57 (s, 1H), 8.85 (dt, *J* = 5.1, 1.5 Hz, 2H), 8.62 (d, *J* = 8.6 Hz, 1H), 8.19 (tt, *J* = 7.7, 1.5 Hz, 1H), 7.92 (dd, *J* = 7.9, 1.4 Hz, 1H), 7.82 (d, *J* = 2.4 Hz, 1H), 7.73 – 7.67 (m, 5H), 7.55 – 7.48 (m, 3H), 7.45 (dd, *J* = 8.4, 7.0 Hz, 2H), 6.99 (d, *J* = 8.7 Hz, 1H), 2.34 (s, 3H) ppm. ^{13}C NMR (100 MHz, DMSO-d_6) δ 161.2, 156.3, 153.0, 152.5, 141.3, 140.0, 135.5, 133.05, 132.8, 132.4, 131.6, 130.9, 130.6, 130.5, 127.6, 126.9, 126.8, 120.8, 120.2, 119.5, 20.0 ppm. HRMS (ESI): Calcd for $C_{24}H_{21}BF_4N_2OPtS$, 679.1052: Found: 592.1026, $[M\text{-}BF_4]^+$.

C3, 81% yield, reddish solid. FT- IR (KBr pellet) cm^{-1}: 3619.3, 3054.3, 1597.2, 1525.4, 1458.3, 1305.1, 1060.1, 820.7, 753.7, 686.7. ^{1}H NMR (500 MHz, DMSO-d_6) δ 9.62 (s, 1H), 8.84 (d, *J* = 5.2 Hz, 2H), 8.57 (d, *J* = 8.6 Hz, 1H), 8.19 (t, *J* = 7.7 Hz, 1H), 7.94 (d, *J* = 7.9 Hz, 1H), 7.85 (dd, *J* = 9.4, 3.0 Hz, 1H), 7.77 – 7.66 (m, 5H), 7.62 (td, *J* = 8.6, 7.9, 3.3 Hz, 1H), 7.57 – 7.50 (m, 2H), 7.45 (t, *J* = 7.7 Hz, 2H), 7.09 (dd, *J* = 9.4, 4.6 Hz, 1H) ppm. ^{13}C NMR (100 MHz, DMSO-d_6) δ 159.5, 157.5, 156.1, 155.2, 152.9, 152.6, 152.5, 141.4, 133.1, 132.8, 132.5, 131.6, 131.0, 130.9, 130.8, 130.3, 127.7, 127.1, 126.9, 126.6, 122.1,

120.2, 119.5, 119.1, 118.8 ppm. HRMS (ESI): Calcd for $C_{24}H_{18}BF_5N_2OPtS$, 683.0801: Found: 596.0700, $[M\text{-}BF_4]^+$.

C4, 83% yield, reddish orange solid. FT- IR (KBr pellet) cm^{-1}: 3059.1, 2920.3, 1602.0, 1515.8, 1444.0, 1386.5, 1314.7, 1070.5, 816.0,758.5, 686.7. ^1H NMR (500 MHz, DMSO-d_6) δ 9.59 (s, 1H), 8.81 (d, *J* = 6.0 Hz, 2H), 8.55 (d, *J* = 8.7 Hz, 1H), 8.23 (s, 1H), 8.18 (t, *J* = 7.8 Hz, 1H), 7.90 (d, *J* = 7.9 Hz, 1H), 7.79 – 7.64 (m, 6H), 7.53 (t, *J* = 7.6 Hz, 2H), 7.44 (t, *J* = 7.7 Hz, 2H), 7.03 (d, *J* = 9.1 Hz, 1H) ppm. ^{13}C NMR (125 MHz, DMSO-d_6) δ 161.6, 156.3, 152.6, 152.6, 141.5, 140.0, 137.8, 133.2, 132.9, 132.5, 131.7, 131.1, 131.03, 130.3, 127.8, 127.3, 122.9, 119.7, 108.6 ppm. HRMS (ESI): Calcd for $C_{24}H_{18}BClF_4N_2OPtS$, 699.0505: Found: 612.0475, $[M\text{-}BF_4]^+$.

C5, 88% yield, light solid. FT- IR (KBr pellet) cm^{-1}: 3633.7, 3054.3, 1592.4, 1511.0, 1386.5, 1309.9, 1161.5, 1060.1, 811.2, 748.9, 686.7. ^1H NMR (400 MHz, DMSO-d_6) δ 9.61 (s, 1H), 8.81 (d, *J* = 5.0 Hz, 2H), 8.55 (d, *J* = 8.5 Hz, 1H), 8.25 (s, 1H), 8.17 (t, *J* = 7.6 Hz, 1H), 7.91 (d, *J* = 7.7 Hz, 1H), 7.72 (dd, *J* = 19.5, 9.8 Hz, 6H), 7.52 (t, *J* = 7.7 Hz, 2H), 7.43 (t, *J* = 7.3 Hz, 2H), 7.02 (d, *J* = 9.1 Hz, 1H) ppm. ^{13}C NMR (100 MHz, DMSO-d_6) δ 161.6, 156.4, 152.6, 141.5, 140.0, 137.8, 133.1, 132.8, 132.5, 131.7, 131.1, 130.9, 130.38, 127.7, 127.3, 122.9, 119.7, 108.5 ppm. HRMS (ESI): Calcd for $C_{24}H_{18}BBrF_4N_2OPtS$, 743.0000: Found: 656.9966, $[M\text{-}BF_4]^+$.

C6, 79% yield, red solid. FT- IR (KBr pellet) cm^{-1}: 3379.9, 3020.8, 1587.6, 1525.4, 1463.1, 1386.5, 1309.9, 1214.2, 1026.6, 825.5, 758.5, 681.9. ^1H NMR (500 MHz, DMSO-d_6) δ 9.55 (s, 1H), 8.81 (s, 2H), 8.58 (d, *J* = 8.2 Hz, 1H), 8.16 (s, 1H), 7.83 (d, *J* = 7.3 Hz, 1H), 7.66 (d, *J* = 6.8 Hz, 5H), 7.50 (q, *J* = 13.8, 10.7 Hz, 3H), 7.43 (t, *J* = 7.4 Hz, 2H), 7.34 (d, *J* = 8.7 Hz, 1H), 7.03 (d, *J* = 9.2 Hz, 1H), 3.78 (s, 3H) ppm. ^{13}C NMR (125 MHz, DMSO-d_6) δ 158.5, 155.8, 153.0, 152.5, 151.1, 141.3, 133.0, 132.8, 132.4, 131.6, 130.9, 130.6, 130.5, 129.2, 127.7, 121.5, 120.1, 119.4, 114.8, 56.0 ppm. HRMS (ESI): Calcd for $C_{25}H_{21}BF_4N_2O_2PtS$, 695.1001: Found: 608.0967, $[M\text{-}BF_4]^+$..

C7, 85% yield, yellow orange solid. FT- IR (KBr pellet) cm^{-1}: 3059.1, 2925.1, 1606.8, 1467.9, 1329.1, 1060.1, 753.7, 691.5. ^1H NMR (500 MHz, DMSO-d_6) δ 9.83 (s, 1H), 9.14 (d, *J* = 3.0 Hz, 1H), 8.82 (d, *J* = 5.6 Hz, 2H), 8.61 (d, *J* = 8.7 Hz, 1H), 8.38 (dd, *J* = 9.5, 2.9 Hz, 1H), 8.20 (t, *J* = 7.8 Hz, 1H), 7.94 (d, *J* = 7.8 Hz, 1H), 7.72 (dt, *J* = 15.6, 7.4 Hz, 5H), 7.55 (q, *J* = 7.3 Hz, 2H), 7.45 (t, *J* = 7.7 Hz, 2H), 7.18 (d, *J* = 9.4 Hz, 1H) ppm. ^{13}C NMR (125 MHz, DMSO-d_6) δ 166.1, 157.8, 152.6, 152.2, 141.7, 138.7, 134.7, 133.3, 132.8, 132.7, 131.8, 131.7, 131.0, 130.1, 127.9, 127.5, 122.0, 120.9, 120.0 ppm. HRMS (ESI): Calcd for $C_{24}H_{18}BF_4N_3O_3PtS$, 710.0746: Found: 623.0722, $[M\text{-}BF_4]^+$.

C8, 87% yield, light orange solid. FT- IR (KBr pellet) cm^{-1}: 3054.3, 1602.0, 1525.4, 1376.9, 1262.0, 1045.8, 825.5, 744.1, 677.1. ^{1}H NMR (500 MHz, DMSO-d_6) δ 9.88 (s, 1H), 8.87 (s, 2H), 8.74 – 8.52 (m, 2H), 8.26 – 8.07 (m, 2H), 7.94 – 7.79 (m, 2H), 7.70 (d, *J* = 6.5 Hz, 6H), 7.53 (t, *J* = 7.4 Hz, 1H), 7.45 (t, *J* = 7.4 Hz, 4H), 7.22 (d, *J* = 9.1 Hz, 1H) ppm. ^{13}C NMR (125 MHz, DMSO-d_6) δ 164.4, 153.7, 152.6, 149.3, 141.4, 139.2, 133.8, 133.1, 132.7, 132.4, 131.6, 131.0, 130.7, 130.1, 129.6, 129.0, 128.1, 127.8, 126.3, 124.8, 122.9, 122.3, 120.0, 112.2 ppm. HRMS (ESI): Calcd for $C_{28}H_{21}BF_4N_3O_3PtS$, 715.1052: Found: 628.1028, $[M\text{-}BF_4]^+$.

4.2. Biology

4.2.1. Cell culture

A549, MCF-7 and HepG2 cancer cells were purchased from ATCC. A549, MCF-7 and HepG2 were maintained in DMEM supplemented with 10% FBS and 1% PEST antibiotics. Cells were grown in CO_2 humidifier having 37 °C.

4.2.2. MTT assay

A549, MCF-7 and HepG2 cancer cells were treated with indicated compounds for 48 h and then analyzed by MTT assay as reported recently by our group [43].

4.2.3. TUNEL assay

A549, MCF-7 and HepG2 cancer cells were treated with indicated compounds for 48 h and then analyzed by TUNEL assay to detect apoptosis using our recently reported method [43].

4.2.4. Clonogenic assay

A549, MCF-7 and HepG2 cancer cells were treated with indicated compounds for 48 h and then cells were grown for next 7 days in drug free DMEM media supplemented with 10% FBS and analyzed using our recently reported method [43].

4.2.5. Western blots data

A549, MCF-7 and HepG2 cancer cells were treated with **C8** for 24 h and treated cells were collected as pellets. Cell lysis and western blot was performed as described previously [43].

4.2.6. Mammosphere assay

A549, MCF-7 and HepG2 cancer cells were grown as tumor sphere/cancer stem cells in ultra-low attachment plates. Tumor sphere/cancer stem cells were treated with **C2**, **C6** and **C8** complexes for 5 days. Mammosphere assay reagents and analysis was performed a reported in our previous manuscript [43].

4.2.7. Invasion assay: Boyden chamber invasion assay

Invasion assay was performed as described previously [64]. BioCoat Matrigel Invasion Chamber was used for A549, MCF-7 and HepG2 cancer cells invasion ability. Briefly, upper chamber were seeded with A549, MCF-7 and HepG2 cancer cells after treatment and the lower chamber contained DMEM supplemented with 10% FBS as a chemoattractant. Then the chamber was incubated in a 5% CO_2 and 37 °C for 24 h. After completion of incubation, A549, MCF-7 and HepG2 cancer cells that were attached with the upper surface of the membrane were wiped very carefully using swab and the A549, MCF-7 and HepG2 invaded cells that were present at the lower surface of the membrane were fixed with formaldehyde for 30 min and then fixed cells were stained with stained with the 0.05% crystal violet solution for 20 min at rt. The invaded cells at the lower chamber after fixing and staining were photographed.

4.2.8. Wound healing assay:

A549, MCF-7 and HepG2 cancer cells were plated at a confluence of 90% and next day wound was performed with 10 µL sterilize tip. Cells were then treated with **C2**, **C6** and **C8** for 24 h and wound healing area was determined after 24 h to detect migration ability of cancer cells.

4.2.9. RT-PCR

HepG2 cells were treated with 20 µM of **C8** for 2 days and then RNA extracted from control and treated cells using trizol reagent. RevertAid™ First Strand cDNA synthesis kit was used to synthesize cDNA from extracted total RNA using the instructions from manufacture protocol. SYBR Green qPCR (Thermo Scientific) was used to analyze mRNA levels by RT-PCR. β-actin: forward: 5-TGGATCAGCAAGCAGGAGTATG-3, reverse: 5-GCATTTGCGGTGGACGAT-3 [65], LDLR: forward: 5'-CCCGACCCCTACCCACTT-3 , reverse: 5-AATAACACAAATGCCAAATGTACACA-3 [65], FASN: Forward: 5-CTTCCGAGATTCCATCCTACGC-3,

Reverse: 5-TGGCAGTCAGGCTCACAAACG-3 [66], HMGCR: Forward: 5-GTTCTGAACTGGAACATGGGC-3, Reverse: 5-TTCATCCTCCACAAGACAATGC-3 [67].

Acknowledgements

The authors acknowledge the Inner Mongolia University funding under the title Academic Backbone (No. 10000-21311201/092) and “JUN-MA” High-level Talents Program of Inner Mongolia University (No. 21300-5195112, No. 21300-5205107).

Appendix A. Supplementary data

Supplementary data, stability figures, ^{1}H, and ^{13}C NMR spectra, HR ESI-MS chromatogram or other related data to this article can be found at http://dx.doi.org/10.

References

[1] S.J. Berners-Price, Activating platinum anticancer complexes with visible light, Angew Chem Int Ed, 50(2011) 804-5.
[2] N.J. Wheate, S. Walker, G.E. Craig, R. Oun, The status of platinum anticancer drugs in the clinic and in clinical trials, Dalton Trans, 39(2010) 8113-27.
[3] N. Cutillas, G.S. Yellol, C. de Haro, C. Vicente, V. Rodríguez, J. Ruiz, Anticancer cyclometalated complexes of platinum group metals and gold, Coord. Chem. Rev., 257(2013) 2784-97.
[4] F.M. Muggia, A. Bonetti, J.D. Hoeschele, M. Rozencweig, S.B. Howell, Platinum antitumor complexes: 50 Years since Barnett Rosenberg's discovery, J Clin Oncol, 33(2015) 4219-26.
[5] B. Rosenberg, L. Vancamp, J.E. Trosko, V.H. Mansour, Platinum compounds - A new class of potent antitumour agents, Nature, 222(1969) 385-6.
[6] B. Rosenberg, L. Vancamp, E.B. Grimley, A.J. Thomson, Inhibition of growth or cell division in *Escherichia Coli* by different ionic species of platinu(IV) complexes, J. Biol. Chem., 242(1967) 1347-52.
[7] B. Rosenberg, E. Renshaw, L. Vancamp, J. Hartwick, J. Drobnik, Platinum induced filamentous growth in *Escherichia Coli*, J. Bacteriol., 93(1967) 716-21.
[8] B. Rosenberg, L. Vancamp, T. Krigas, Inhibition of cell division in *Escherichia Coli* by electrolysis products from a platinum electrode, Nature, 205(1965) 698-9.
[9] B.W. Harper, A.M. Krause-Heuer, M.P. Grant, M. Manohar, K.B. Garbutcheon-Singh, J.R. Aldrich-Wright, Advances in platinum chemotherapeutics, Chem. Eur. J., 16(2010) 7064-77.
[10] R.E. Windsor, S.J. Strauss, C. Kallis, N.E. Wood, J.S. Whelan, Germline genetic polymorphisms may influence chemotherapy response and disease outcome in osteosarcoma, Cancer, 118(2012) 1856-67.
[11] N. Milosavljevic, C. Duranton, N. Djerbi, P.H. Puech, P. Gounon, D. Lagadic-Gossmann, et al., Nongenomic effects of cisplatin: acute inhibition of mechanosensitive transporters and channels without actin remodeling, Cancer Res., 70(2010) 7514-22.
[12] P.J. Loehrer, L.H. Einhorn, Cisplatin, Ann. Intern. Med., 100(1984) 704-13.
[13] R.S.A. J A Levi, D N Dalley, Haemolytic anemia after cisplatin, Br. Med. J., 282(1981) 2003–4.
[14] L. Dvořák, I. Popa, P. Štarha, Z. Trávníček, In Vitro Cytotoxic-Active Platinum(II) Complexes Derived from Carboplatin and Involving Purine Derivatives, Eur. J. Inorg. Chem., 2010(2010) 3441-8.
[15] P. Virag, M. Perde-Schrepler, E. Fischer-Fodor, C. Tatomir, S.A. Dorneanu, V.I. Cernea, et al., Superior cytotoxicity and DNA cross-link induction by oxaliplatin versus cisplatin at lower cellular uptake in colorectal cancer cell lines, Anti-Cancer Drugs, 23(2012) 1032-8.

[16] S.E. Sherman, S.J. Lippard, Structural aspects of platinum anticancer drug interactions with DNA, Chem. Rev., 87(1987) 1153-81.
[17] F. Arnesano, G. Natile, Mechanistic insight into the cellular uptake and processing of cisplatin 30 years after its approval by FDA, Coord. Chem. Rev., 253(2009) 2070-81.
[18] F.U. Rahman, A. Ali, I.U. Khan, H.Q. Duong, R. Guo, H. Wang, et al., Novel phenylenediamine bridged mixed ligands dimetallic square planner Pt(II) complex inhibits MMPs expression via p53 and caspase-dependent signaling and suppress cancer metastasis and invasion, Eur. J. Med. Chem., 125(2017) 1064-75.
[19] D. Smilowicz, N. Metzler-Nolte, Synthesis of monofunctional platinum(iv) carboxylate precursors for use in Pt(iv)-peptide bioconjugates, Dalton Trans, (2018).
[20] A. Gornowicz, A. Bielawska, W. Szymanowski, H. Gabryel-Porowska, R. Czarnomysy, K. Bielawski, Mechanism of anticancer action of novel berenil complex of platinum(II) combined with anti-MUC1 in MCF-7 breast cancer cells, Oncol Lett, 15(2018) 2340-8.
[21] T.C. Johnstone, K. Suntharalingam, S.J. Lippard, The next generation of platinum drugs: targeted Pt(II) agents, nanoparticle delivery and Pt(IV) prodrugs, Chem Rev, 116(2016) 3436-86.
[22] W. Zhou, M. Almeqdadi, M.E. Xifaras, I.A. Riddell, O.H. Yilmaz, S.J. Lippard, The effect of geometric isomerism on the anticancer activity of the monofunctional platinum complex trans-$[Pt(NH_3)_2$(phenanthridine)Cl]NO_3, Chem Commun (Camb), 54(2018) 2788-91.
[23] T.C. Johnstone, G.Y. Park, S.J. Lippard, Understanding and improving platinum anticancer drugs--phenanthriplatin, Anticancer Res., 34(2014) 471-6.
[24] T.C. Johnstone, S.J. Lippard, The chiral potential of phenanthriplatin and its influence on guanine binding, J. Am. Chem. Soc., 136(2014) 2126-34.
[25] T.C. Johnstone, S.M. Alexander, W. Lin, S.J. Lippard, Effects of monofunctional platinum agents on bacterial growth: a retrospective study, J. Am. Chem. Soc., 136(2014) 116-8.
[26] S. Kemp, N. Wheate, S. Wang, J.G. Collins, S. Ralph, A. Day, et al., Encapsulation of platinum(II)-based DNA intercalators within cucurbit[6,7,8]urils, J. Biol. Inorg. Chem., 12(2007) 969-79.
[27] S. Roy, K.D. Hagen, P.U. Maheswari, M. Lutz, A.L. Spek, J. Reedijk, et al., Phenanthroline derivatives with improved selectivity as DNA-targeting anticancer or antimicrobial drugs, ChemMedChem, 3(2008) 1427-34.
[28] R.G. Kenny, C.J. Marmion, Toward multi-targeted platinum and ruthenium drugs-A new Paradigm in cancer drug treatment regimens?, Chem Rev, 119(2019) 1058-137.
[29] A.G. Quiroga, M. Cama, N. Pajuelo-Lozano, A. Alvarez-Valdes, I. Sanchez Perez, New findings in the signaling pathways of *cis* and *trans* platinum iodido complexes interaction with DNA of cancer cells, ACS Omega, 4(2019) 21855-61.
[30] L. Ma, X. Lin, C. Li, Z. Xu, C.-Y. Chan, M.-K. Tse, et al., A cancer cell-selective and low-toxic bifunctional heterodinuclear Pt(IV)–Ru(II) anticancer prodrug, Inorganic Chemistry, 57(2018) 2917-24.
[31] D. Guo, E.H. Bell, P. Mischel, A. Chakravarti, Targeting SREBP-1-driven lipid metabolism to treat cancer, Curr. Pharm. Des., 20(2014) 2619-26.
[32] C.V. Dang, A. Le, P. Gao, MYC-induced cancer cell energy metabolism and therapeutic opportunities, Clin. Cancer. Res., 15(2009) 6479-83.
[33] Y.A. Wen, X. Xiong, Y.Y. Zaytseva, D.L. Napier, E. Vallee, A.T. Li, et al., Downregulation of SREBP inhibits tumor growth and initiation by altering cellular metabolism in colon cancer, Cell death & disease, 9(2018) 265.
[34] F. Yin, F. Feng, L. Wang, X. Wang, Z. Li, Y. Cao, SREBP-1 inhibitor Betulin enhances the antitumor effect of Sorafenib on hepatocellular carcinoma via restricting cellular glycolytic activity, Cell death & disease, 10(2019) 672.
[35] J. Li, H. Yan, L. Zhao, W. Jia, H. Yang, L. Liu, et al., Inhibition of SREBP increases gefitinib sensitivity in non-small cell lung cancer cells, Oncotarget, 7(2016) 52392-403.
[36] J. Fares, M.Y. Fares, H.H. Khachfe, H.A. Salhab, Y. Fares, Molecular principles of metastasis: a hallmark of cancer revisited, Signal Transduct Target Ther, 5(2020) 28.

[37] W.G. Jiang, A.J. Sanders, M. Katoh, H. Ungefroren, F. Gieseler, M. Prince, et al., Tissue invasion and metastasis: Molecular, biological and clinical perspectives, Semin. Cancer Biol., 35 Suppl(2015) S244-S75.
[38] L.T.H. Phi, I.N. Sari, Y.G. Yang, S.H. Lee, N. Jun, K.S. Kim, et al., Cancer stem cells (CSCs) in drug resistance and their therapeutic implications in cancer treatment, Stem Cells Int, 2018(2018) 5416923.
[39] E. Currie, A. Schulze, R. Zechner, T.C. Walther, R.V. Farese, Jr., Cellular fatty acid metabolism and cancer, Cell Metab, 18(2013) 153-61.
[40] R.A. Cairns, I. Harris, S. McCracken, T.W. Mak, Cancer cell metabolism, Cold Spring Harb Symp Quant Biol, 76(2011) 299-311.
[41] M. Patra, T.C. Johnstone, K. Suntharalingam, S.J. Lippard, A Potent Glucose-Platinum Conjugate Exploits Glucose Transporters and Preferentially Accumulates in Cancer Cells, Angew. Chem. Int. Ed. Engl., 55(2016) 2550-4.
[42] C. Li, F. Xu, Y. Zhao, W. Zheng, W. Zeng, Q. Luo, et al., Platinum(II) terpyridine anticancer complexes possessing multiple mode of DNA interaction and EGFR inhibiting activity, Front Chem, 8(2020) 210.
[43] X. Bai, A. Ali, Z. Lv, N. Wang, X. Zhao, H. Hao, et al., Platinum complexes inhibit HER-2 enriched and triple-negative breast cancer cells metabolism to suppress growth, stemness and migration by targeting PKM/LDHA and CCND1/BCL2/ATG3 signaling pathways, Eur. J. Med. Chem., 224(2021) 113689.
[44] F.U. Rahman, A. Ali, H.Q. Duong, I.U. Khan, M.Z. Bhatti, Z.T. Li, et al., ONS-donor ligand based Pt(II) complexes display extremely high anticancer potency through autophagic cell death pathway, Eur. J. Med. Chem., 164(2019) 546-61.
[45] F.-U. Rahman, A. Ali, M.Z. Bhatti, Z.-T. Li, H. Wang, D.-W. Zhang, Synthesis, single crystal X-ray structures of ONNO, ONN and ONS-Pd(II) complexes and their anticancer activities, Chem. Dat. Collect., 19(2019).
[46] F.U. Rahman, M.Z. Bhatti, A. Ali, H.Q. Duong, Y. Zhang, B. Yang, et al., Homo- and heteroleptic Pt(II) complexes of ONN donor hydrazone and 4-picoline: A synthetic, structural and detailed mechanistic anticancer investigation, Eur. J. Med. Chem., 143(2017) 1039-52.
[47] F.U. Rahman, A. Ali, I.U. Khan, H.Q. Duong, S.B. Yu, Y.J. Lin, et al., Morpholine or methylpiperazine and salicylaldimine based heteroleptic square planner platinum (II) complexes: *In vitro* anticancer study and growth retardation effect on *E. coli*, Eur. J. Med. Chem., 131(2017) 263-74.
[48] F.-U. Rahman, A. Ali, I.U. Khan, H.-Q. Duong, R. Guo, H. Wang, et al., Novel phenylenediamine bridged mixed ligands dimetallic square planner Pt(II) complex inhibits MMPs expression via p53 and caspase-dependent signaling and suppress cancer metastasis and invasion, Eur. J. Med. Chem., 125(2017) 1064-75.
[49] F.-U. Rahman, A. Ali, I. Khan, R. Guo, L. Chen, H. Wang, et al., Synthesis and characterization of *trans*-Pt(II)(salicylaldimine)(pyridine/pyridine-4-carbinol)Cl complexes: *In vivo* inhibition of *E. coli* growth and *in vitro* anticancer activities, Polyhedron, 100(2015) 264-70.
[50] F.-U. Rahman, A. Ali, R. Guo, Y.-C. Zhang, H. Wang, Z.-T. Li, et al., Synthesis and anticancer activities of a novel class of mono- and di-metallic Pt(II)(salicylaldiminato)(DMSO or picolino)Cl complexes, Dalton Trans, 44(2015) 2166-75.
[51] F.U. Rahman, A. Ali, R. Guo, W.K. Wang, H. Wang, Z.T. Li, et al., Efficient one-pot synthesis of trans-Pt(II)(salicylaldimine)(4-picoline)Cl complexes: effective agents for enhanced expression of p53 tumor suppressor genes, Dalton Trans, 44(2015) 9872-80.
[52] M.D. Hall, K.A. Telma, K.E. Chang, T.D. Lee, J.P. Madigan, J.R. Lloyd, et al., Say no to DMSO: dimethylsulfoxide inactivates cisplatin, carboplatin, and other platinum complexes, Cancer Res., 74(2014) 3913-22.
[53] J. Reedijk, Platinum anticancer coordination compounds: study of DNA binding inspires new drug design, Eur. J. Inorg. Chem., 2009(2009) 1303-12.
[54] S. Ahmad, Kinetic aspects of platinum anticancer agents, Polyhedron, 138(2017) 109-24.

[55] C.M. Clavel, E. Păunescu, P. Nowak-Sliwinska, A.W. Griffioen, R. Scopelliti, P.J. Dyson, Modulating the anticancer activity of ruthenium(II)–arene complexes, J. Med. Chem., 58(2015) 3356-65.
[56] L. Cubo, D.S. Thomas, J. Zhang, A.G. Quiroga, C. Navarro-Ranninger, S.J. Berners-Price, [^{1}H,^{15}N] NMR studies of the aquation of *cis*-diamine platinum(II) complexes, Inorg. Chim. Acta, 362(2009) 1022-6.
[57] G.Y. Park, J.J. Wilson, Y. Song, S.J. Lippard, Phenanthriplatin, a monofunctional DNA-binding platinum anticancer drug candidate with unusual potency and cellular activity profile, PNAS, 109(2012) 11987-92.
[58] G. Zhu, M. Myint, W.H. Ang, L. Song, S.J. Lippard, Monofunctional platinum-DNA adducts are strong inhibitors of transcription and substrates for nucleotide excision repair in live mammalian cells, Cancer Res., 72(2012) 790-800.
[59] N. Koundouros, G. Poulogiannis, Reprogramming of fatty acid metabolism in cancer, Br. J. Cancer, 122(2020) 4-22.
[60] M. Chen, J. Huang, The expanded role of fatty acid metabolism in cancer: new aspects and targets, Precis Clin Med, 2(2019) 183-91.
[61] X. Luo, C. Cheng, Z. Tan, N. Li, M. Tang, L. Yang, et al., Emerging roles of lipid metabolism in cancer metastasis, Mol Cancer, 16(2017) 76.
[62] O.V. Dolomanov, L.J. Bourhis, R.J. Gildea, J.A.K. Howard, H. Puschmann, OLEX2: a complete structure solution, refinement and analysis program, J. Appl. Crystallogr., 42(2009) 339-41.
[63] D. Kratzert, J.J. Holstein, I. Krossing, DSR: enhanced modelling and refinement of disordered structures with SHELXL, J. Appl. Crystallogr., 48(2015) 933-8.
[64] K.H. Shen, J.H. Hung, Y.C. Liao, S.T. Tsai, M.J. Wu, P.S. Chen, Sinomenine inhibits migration and invasion of human lung cancer cell through downregulating expression of miR-21 and MMPs, Int J Mol Sci, 21(2020) 3080.
[65] S. Adachi, M. Homoto, R. Tanaka, Y. Hioki, H. Murakami, H. Suga, et al., ZFP36L1 and ZFP36L2 control LDLR mRNA stability via the ERK-RSK pathway, Nucleic Acids Res., 42(2014) 10037-49.
[66] J. Li, L. Dong, D. Wei, X. Wang, S. Zhang, H. Li, Fatty acid synthase mediates the epithelial-mesenchymal transition of breast cancer cells, Int J Biol Sci, 10(2014) 171-80.
[67] J.W. Clendening, A. Pandyra, P.C. Boutros, S. El Ghamrasni, F. Khosravi, G.A. Trentin, et al., Dysregulation of the mevalonate pathway promotes transformation, Proc Natl Acad Sci U S A, 107(2010) 15051-6.